ICAS 2021 SHANGHAI
International Council of the Aeronautical Sciences
32nd Congress of the International Council of the Aeronautical Sciences
September 6-10, 2021
Pudong Shangri-La, Shanghai, China

NUMERICAL SIMULATIONS OF TRANSONIC BUFFET ON A HALF WING-BODY CONFIGURATION

Fulvio Sartor[1], Michaël Martin[1], Carmen Riveiro Moreno[1] & Julien Dandois[1]

[1]ONERA, DAAA. 8 rue des Vertugadins. 92190 Meudon, France

Abstract

At cruise conditions, the flow around a civil aircraft is characterised by shock waves, interacting with the boundary layer developing over the wing. A strong interaction may lead to significant separation, causing large-scale unsteadiness, such as high-amplitude self-sustained shock movements, known as transonic buffet. This phenomenon presents an industrial interest and can be observed both on two- and three-dimensional configurations. When considering 3D wings, limited results have been published by numerical simulations. Some authors have successfully applied RANS approaches, but recent works have also shown that unsteady Reynolds-averaged Navier-Stokes equations can be used to reproduce the shock unsteadiness. The study proposed in this article will consist in performing steady (RANS) and unsteady (both URANS and ZDES) simulations of the flow around a half wing-body configuration at transonic speed. The investigations will focus on the buffet unsteadiness, its onset, and the flow conditions that can cause the shock instability. Validation is performed thanks to comparisons with an experimental database available at ONERA, which has played a central role in buffet research over the last 30 years.

Keywords: transonic buffet, URANS, ZDES

1. Introduction

Transonic buffet is one of the critical unsteady phenomena that limit the flight envelope of an aircraft, occurring for specific combinations of flow Mach numbers and angles of attack. This unsteady phenomenon is an aerodynamic excitation characterised by self-sustained displacements of the shock wave location and periodic boundary-layer separation downstream from the shock. The correct prediction of this unsteady shock-wave/boundary-layer interaction is a challenging problem for CFD. Moreover, the experimental data that are available for code validation are very limited.

1.1 The transonic buffet phenomenon

Ever since first observed, the scientific community has put great effort to understand the physical mechanism underlying buffet and its onset. Depending on the configuration, buffet can display a 2D or 3D nature. Given their differences, the transonic buffet phenomenon can be divided into two categories: buffet on 2D aerofoils and buffet on 3D airplane wings. On a first place, research focused on transonic buffet on aerofoils, purely 2D, which is well documented nowadays. Later on, transonic buffet on wings was considered and found to be a 3D complex phenomenon whose physical mechanism was not fully understood. For both cases, experimental campaigns and CFD simulations have been carried out to seek a better understanding.

Although the buffet phenomenon on an aerofoil is essentially 2D, Jacquin [1] already noticed that for a rectangular constant cross section wing 3D weak instabilities were present. As the wing differs from this configuration during buffeting, the 3D effects become dominant. As a result, the buffet over an airplane wing which is often swept, twisted and tapered, displays a 3D nature, showing some differences with respect to its 2D version. As a consequence, transonic buffet on a 3D wing can be much more complex than the periodic chord-wise motion observed on 2D profiles.

Buffet over a wing, as its version over an aerofoil, predominantly consists in a periodic self-sustained motion of the shock, result of an unsteady separated boundary layer. This phenomenon takes place

for given combinations of angles of attack and Mach numbers. Therefore, the existence of a separated unsteady boundary layer does not imply the existence of buffet. However, contrary to 2D buffet, the motion of the shock does not correspond with an isolated peak in the spectrum but with a broadband bumps at Strouhal numbers 4 and 7 times higher [2, 3, 4]. As the analysis of the experimental data performed by Dandois shows [4], these Strouhal numbers are within the range $0.2 < St < 0.6$. In addition to this phenomenon, the Kelvin-Helmholtz instability, also present in the 2D buffet [5], ranging between $1 < St < 4$ is also found on the suction side of the wing. Another characteristic of the swept wing buffet is that the shock unsteadiness often first emerges at the wingtip and progresses inboard with increasing angle of attack. However, this feature depends on the wing twist and different behaviours can be observed in other wings.
An explanation for the differences arising between the 2D and 3D buffet phenomena can be attributed to a span-wise propagation of the so called “buffet cells” introduced by Iovnovich and Raveh [6]. Experiments on the CRM by Koike et al. [7] found that these span-wise undulations originated near the wing root and propagated outboard towards the tip, at a convection speed that decreases with an increase in angle of attack. These motions have been the subject of numerous studies in recent years. Crouch [8], Paladini [9] and Plante [10, 11] were able to link the presence of these motions to the superposition of two global instabilities (buffet and stall cells). Moreover, the convection of those cells towards the wing tip has been related to the wing sweep angle.

1.2 State of the art of buffet simulation

Numerous numerical studies seeking a correct prediction of the 3D buffet by means of CFD have been carried out in the past decades. Being the least computational costly, RANS has been able to successfully predict buffet onset [12]. Nonetheless, due to its steady nature, no unsteady information on the buffet itself can be obtained. Sartor and Timme [13] used an URANS approach to reproduce the dominant flow features. This was feasible since shock motions occur at time scales that are much larger than those of the wall-bounded turbulence. However, the result is strongly dependent on the turbulence model and the angle of attack has to be increased with respect to the experimental one. Moreover, different authors [14, 15] pointed out that scale-resolving provides a better agreement with experimental data. For instance, DDES and ZDES are capable of capturing a rich turbulent spectrum of the structures being shed away from the shock foot and DDES yields the right curvature of the outboard mean shock foot trace.
This paper presents some results of an investigation that aims at answering some of the questions that still remain unanswered in the domain of buffet simulation in order to validate the CFD codes and assess the current unsteady CFD methods for the buffet prediction. This paper proceeds as follow: after a brief presentation of the well-known CAT3D model and the experimental data available, the results of the steady-state RANS simulations are first presented. Then, results of the time-accurate simulations are discussed and validated against the experimental data: first URANS simulations, then the turbulence-resolving ZDES approach using the latest improvement of the mode 2 [17], which allows for an automatic switch between RANS and LES and an extended protection to the grid-induced separation. The lessons learnt and the best-practices for future simulations are summarised in the conclusion.

2. The test case: ONERA CAT3D model

All the calculations will be conducted on the same geometry, which was created at ONERA and has been used in the EU-funded AVERT “Aerodynamic Validation of Emission Reducing Technologies” project launched in 2007 and coordinated by Airbus Operations Ltd. The model was named CAT3D and consists in a half-model geometry composed of a wing and fuselage.

2.1 CAT3D geometry

The test case is depicted in figure 1: the wing section is based on the OAT15A supercritical profile which has a thickness to chord ratio of 12.5% and a thick trailing edge of 0.5% of the chord length. The wing span of the CAT3D model is 1.225 m and the wing sweep angle is 30^o. The mean aerodynamic chord is 0.3375 m with a maximum value of 0.450m at the wing root and a minimal value of 0.225 m

at the wing tip. The wing twist was adapted to ensure that the shock remains parallel to the leading edge.

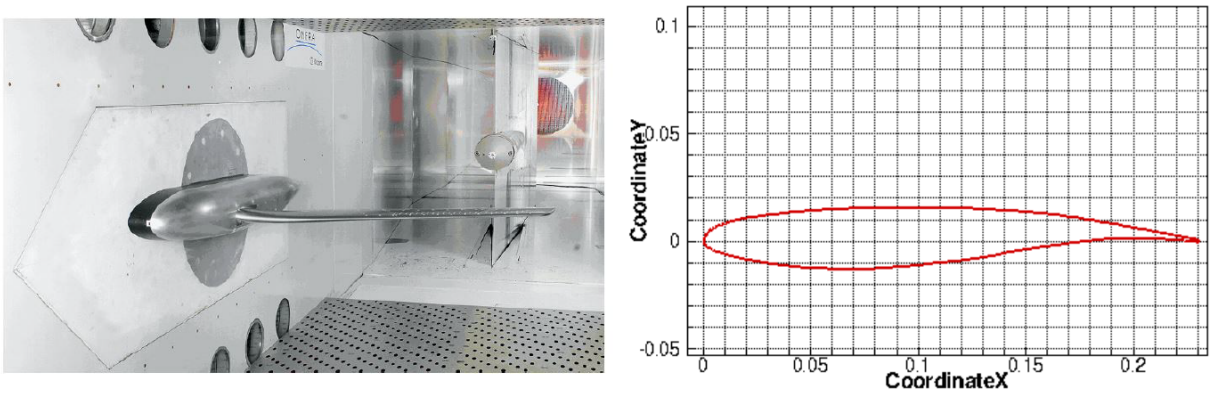

Figure 1 – CAT3D model in the ONERA S2MA wind tunnel (left) and OAT15A profile (right)

2.2 The experimental database

The database used for validation of the simulations presented in this work corresponds to the experimental campaign performed in ONERA S2MA wind tunnel, result of the EU-funded AVERT project. Only a part of this database is used to validate the results presented in this work.

The experimental campaign was conducted in the ONERA S2MA wind tunnel, a continuous pressurised subsonic, transonic and supersonic wind tunnel. Its test section of 1.75 m by 1.77 m, allows the use of relatively large models, such as the CAT3D. So as to study the transonic buffet, the model was equipped with 86 steady pressure taps distributed over 4 wing sections, 65 on the upper surface and 21 on the lower surface of the wing. Additionally, 57 unsteady transducers spread over 7 wing sections, 53 on the upper surface and 4 on the lower surface of the wing were included. Additionally, 6 accelerometers on 3 wing sections, 2 per wing section, were installed as illustrated in figure 2.

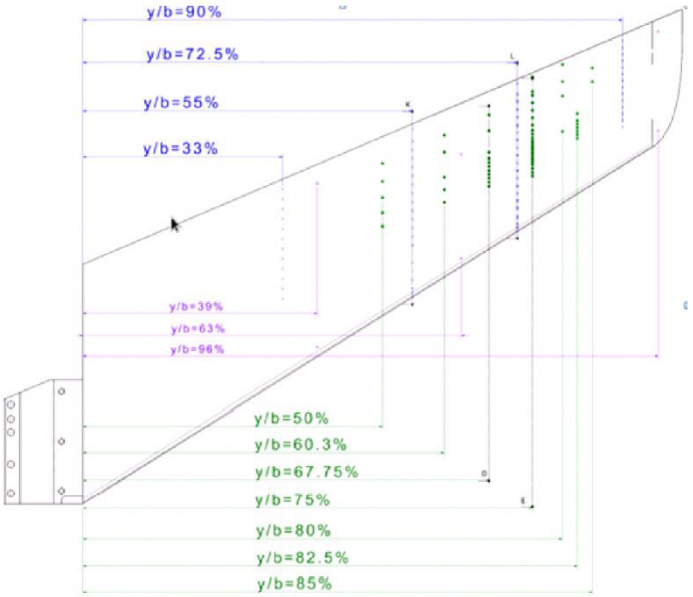

Figure 2 – Model equipment: static pressure taps in blue, unsteady pressure transducers in green, accelerometers in purple

The test conditions are presented in table 1. All simulations use the same conditions for the domain boundaries: non reflective condition on the far-field and adiabatic walls on the model surface.

	Mach Number	AoA α	Total Pressure	Total Temperature	Reynolds Number
Steady conditions	0.826	2.54°	60,000 Pa	293 K	2.84e+6
Unsteady conditions	0.826	4.22°	60,000 Pa	293 K	2.84e+6

Table 1 – Test conditions for the two considered points

2.3 Numerical grids

For this study two grids were employed: a baseline grid, already considered in previous studies for RANS and URANS simulations, and a refined grid, designed for the ZDES simulations and thus allowing the resolution of turbulence in the buffet region. The baseline grid has been created using ICEM CFD software while the refined one has been obtained using Pointwise and the chimera technique. The details of each grid are presented in the next sections.

3. Results of the RANS and URANS simulations

This part describes the results obtained by means of RANS and URANS simulations. All simulations were performed with the ONERA-Airbus-SAFRAN elsA software, whose developments are partially funded by Airbus, Safran, and ONERA which are co-owners of this software [16]. Despite the always growing capabilities for high-performance simulation, industrial mid-fidelity approaches like RANS simulations are still of interest. The literature on URANS simulations of transonic buffet phenomenon on half wing-fuselage configurations is relatively limited. Contrarily to what was believed in the beginning of the 2000s [14], URANS simulations are able to reproduce transonic buffet with modern codes. However, best practices are still not available and some questions remain unanswered. In this section the authors aim at determining the best practices that enable URANS simulations to properly describe the physics of the buffet phenomenon. The influence of turbulence model and numerical scheme is investigated, and the results of the numerical simulations are compared with experimental data for validation.

3.1 RANS grid

All the simulations presented in this section have been performed on the same grid which was already used in previous studies. The computational domain is a multi-blocks H-type structured grid split over 112 processors of ONERA's HPC. The mesh is composed of approximately 5.2 M points and the distribution over HPC's processors assigns an average of 52,000 points per processor, giving a maximum balancing rate of 2.8% which is low enough for good performances.

3.2 Steady-state simulations

The results will be presented for the selected turbulence models: Spalart-Allmaras, k-ω of Menter with SST correction, k-ω of Wilcox and k-kL. For each model, numerical schemes of Roe, Jameson and AUSM+P are considered. The objective is to validate the assumption that the crucial parameter for buffet prediction is the turbulence model, and to evaluate the consistency between these simulations and experimental data.

Residual convergence was achieved at low incidence, with density residuals decreasing by at least 5 orders of magnitude. Depending on the turbulence model and numerical scheme, residuals may present some oscillations but no conclusion can be drawn from this observation: no clear link can be found between the non-convergence of a simulation and the presence of buffet unsteadiness. At high angle of attack, residuals do not present the same level of convergence, which could either be caused by the presence of flow unsteadiness, or by some convergence issues in the simulation.

Figure 3 presents the evolution of the lift coefficient during the iterations: the purple line indicates the experimental value of the lift as measured in the wind tunnel test. At low angle of attack incidence, computations predict values of the lift coefficient slightly higher than the experimental tests, but the agreement is satisfying. In particular, the result obtained with the k-kL turbulence model and Roe scheme yields a lift coefficient of 0.590, which is 0.3% off the experimental value 0.588. In general, all results obtained with the k-kL model (for all schemes) or the Roe scheme (for all models) produce

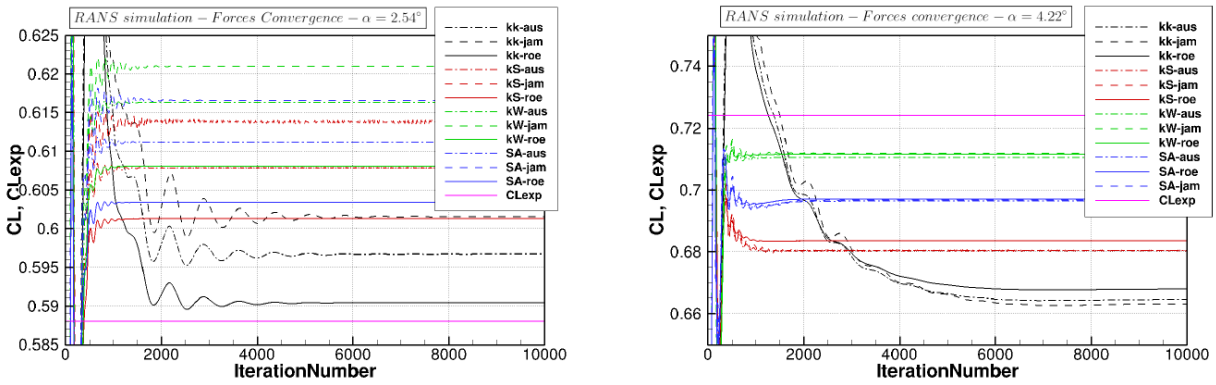

Figure 3 – Lift coefficient for the low (left side, α=2.54^o) and high (right side, α=4.22^o angle of attack

a satisfying agreement. On the contrary, results obtained with the k-ω of Wilcox model yields the least satisfying agreement, regardless the numerical scheme, with a discrepancy with respect to the experimental value up to 5.6% (C_L = 0.621 for kW-jam versus 0.588 from the experiments). When focusing on the higher angle of attack (right part of figure 3), the general behaviour just described is the opposite: k-kL turbulence model underpredicts the most the lift coefficient, while k-ω of Wilcox is the model that yields the most correct prediction. The agreement with the experimental results is generally less satisfying than in the low-incidence case, with an underestimation of the lift coefficient of at least 2% (C_L = 0.710 for the k-ω of Wilcox with Jameson scheme vs 0.724 in the experiments). The major impact on the lift value comes from the turbulence model, while the numerical scheme has a secondary but not negligible effect. It is interesting to notice that for the k-kL turbulence model the convergence is slower because it was not possible to use multi-grid technique, and also that for the other cases, a converged solution is obtained in less than 3,000 iterations.
Pressure-coefficient distributions were evaluated on four span locations, starting from a near fuselage position, where a lambda shock pattern should be observed, to the wing tip where shock oscillations are more likely to occur. Figure 4 shows the location of these slices plotted on skin friction magnitude contour at α = 2.54^o. These positions correspond to the location of pressure taps during experimental investigations.

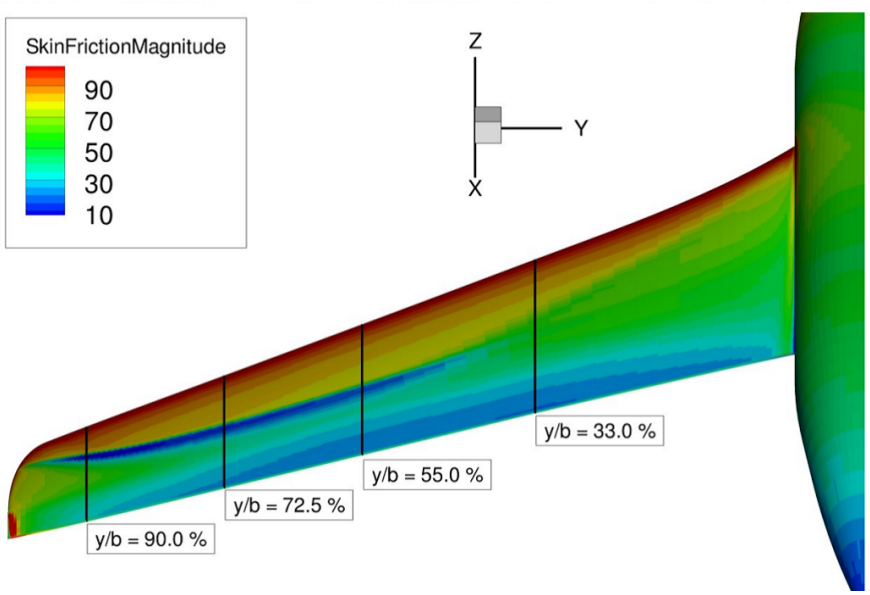

Figure 4 – Magnitude of the skin friction coefficient at low angle of attack (α=2.54^o). Solid black lines indicate the location of the 4 span-wise sections where pressure distributions are analysed and compared with experimental data

Figure 5 shows the pressure distribution at y/b = 33.0% and y/b = 72.5% of the wing span for the

two selected incidences. At low angle of attack, RANS simulations fail to predict the lambda shock pattern: on the fuselage at y/b = 33.0%, experimental data clearly show the presence of two shocks forming the lambda pattern, while simulations predict that these two shocks merged at a location closer to the fuselage (approximately 26% of the wing span).
These differences could come from the laminar-turbulent transition point, as discussed in the next section. However, with the exception of the position of the intersection of the two shocks in the near fuselage area, all RANS simulations predict very well the average position of the shock at other wing span positions, even if few differences arise from the choice of the turbulence model. In this Mach number - angle of attack domain (which is below the buffet onset boundary), steady state simulations enable to properly capture the flow physics of the flow.

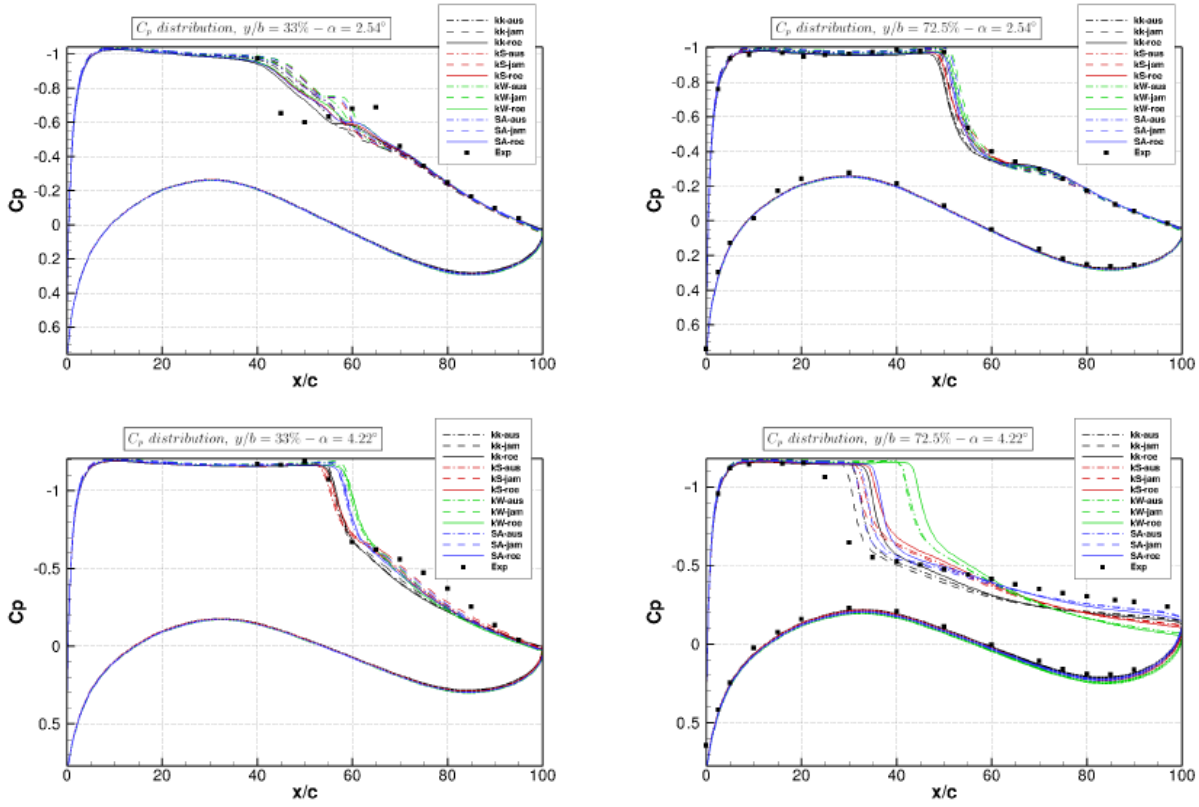

Figure 5 – Pressure coefficient distribution at two span-wise locations (y/b = 33% on the left, y/b = 72.5% on the right) for the low and high angle of attack (top and bottom figures, respectively)

For the high incidence case, α = 4.22º, still in figure 5, the two shocks from the lambda pattern merge at a position closer to the fuselage, this is why pressure taps located at y/b = 33% of the span do not account for a lambda shock pattern. At this location, pressure distributions predicted by numerical simulations are in good agreement with the experimental ones observed experimentally, even if differences between turbulence models increased compared to the low incidence case. However, for a location closer to the wing tip, all numerical simulations fail to predict the shock position and the turbulence model has a major influence on this location. The same conclusions can be drawn from the pressure distribution at y/b = 55% and y/b = 90%. Even if some turbulence models (i.e k-kL) predicts a shock position closer to the experimental value than others (i.e. k-ω of Wilcox), none of the steady state results can reproduce the correct shock position in all span-wise locations. This could be the evidence that unsteady phenomena exist in this region of the span, making steady-state RANS simulations unsuitable for this type of flow: time-accurate simulations could be more suitable to properly capture the flow physics.

Sensitivity to transition and wing deformation

Steady-state simulations are used to investigate the dependency to boundary-layer transition and wing deformation. In the previous section flow was assumed fully turbulent. However, in the experi-

mental conditions, turbulence transition was triggered at 7% of the wing and 20 mm from the fuselage nose. Steady-state simulations were thus performed triggering turbulence transition at the same location as in experiments, using the Spalart-Allmaras turbulence model along with AUSM+P numerical schemes. The choice of this combination of model and scheme was mainly due to the robustness of the solution. Figure 6 shows that triggering the transition has little influence on pressure distribution. A laminar region in the leading edge of the wing is responsible for moving the shock to a slightly more rearward position. However, the differences between numerical and experimental results in the lambda shock pattern are still present.

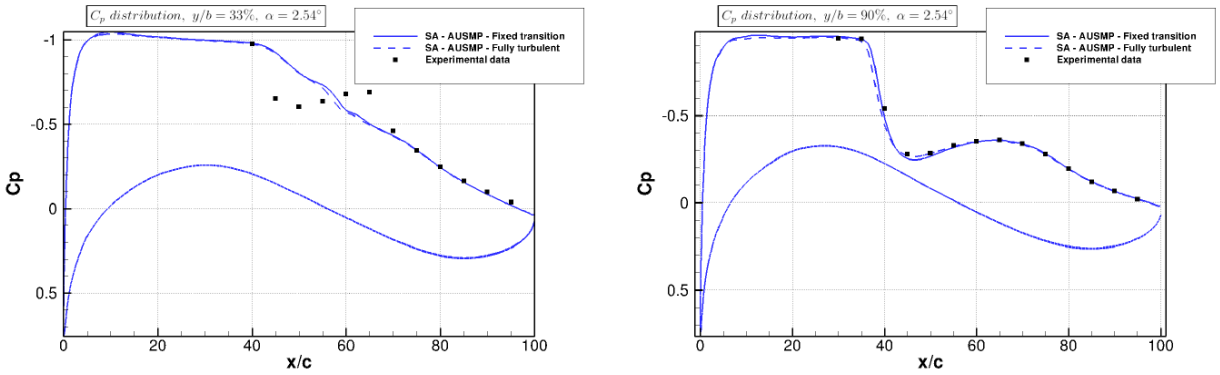

Figure 6 – Cp distributions with and without turbulent transition at two span-wise locations: close to the fuselage (y/b = 33% in the left plot) and close to the wing tip (right image for y/b = 90%)

Despite the rigid material composing the model tested in the wind tunnel, the geometry is slightly deformed due to the loads, especially in the wing tip region. Optical methods enable to accurately measure static deformation of the wing, whose main effects is to increase the twisting (thus lowering the local incidence in the wing-tip region) and to increase the bending. Cp distributions with and without taking into the account the model deformation are compared in figure 7.

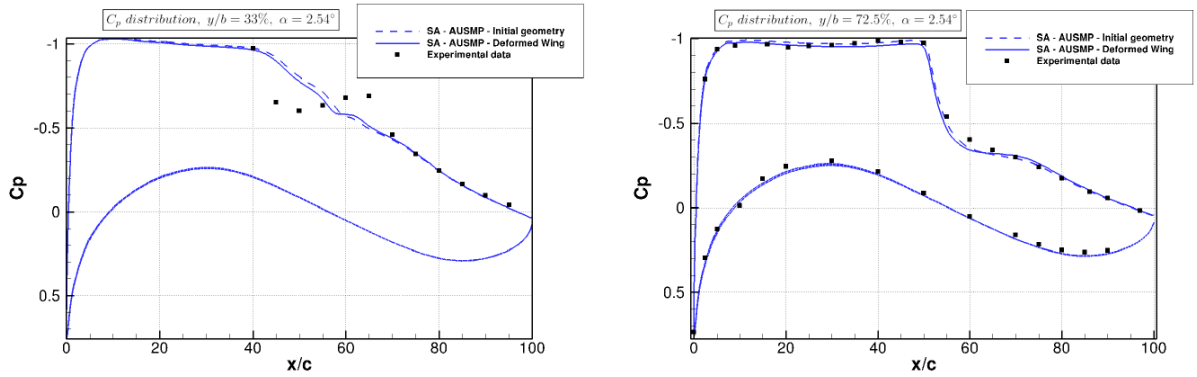

Figure 7 – Cp distribution with and without wing deformation at two span-wise locations: close to the fuselage (y/b = 33% in the left plot) and close to the wing tip (right image for y/b = 72.5%)

As it can be seen from the plot, static deformation tends to move the shock to a forward position. At y/b = 33% the Cp of the deformed model yields a better comparison with the experimental data: a double pressure drop appears close to the fuselage. For the other span locations (y/b = 72.5% for example, as in the right side of in Figure 7), there are very few differences between the computed Cp distributions. For the high angle of attack, not shown in the figure, the influence of the deformation is very limited near to the wing root, but increases near to the wing tip. Overall, taking into account the effect of the static deformation of the wing does not enable to improve consistency of the steady state results with experimental data.

3.3 Time-accurate simulations

Steady-state simulations yield a correct representation of a flow only in absence of unsteadiness. For higher angles of attack, the presence of the buffet phenomenon implies the necessity of time-accurate simulations, presented in this section. The sensitivity with respect to some modelling and numerical parameters has been investigated.

Concerning the temporal discretisation, it has been found that the Gear's formulation with a time step of 1e-5 seconds and 12 inner iterations provided the best compromise between accuracy and computational cost. Decreasing the time step or increasing the number of inner iterations did not improve the accuracy of the results despite increasing the CPU time needed for the simulation of one buffet cycle. On the contrary, one could speed up the simulations by using a larger time step or increasing the number of inner iterations, but the result will be less accurate: the convergence of the inner-iteration would be lower and the coarser time discretisation would damp the shock-oscillation amplitudes.

As done in the previous section for steady-state results, a wide combination of turbulence models and numerical schemes has been considered to investigate the dependency of those parameters. Figure 8 shows the evolution of the lift coefficient for all the considered simulations.

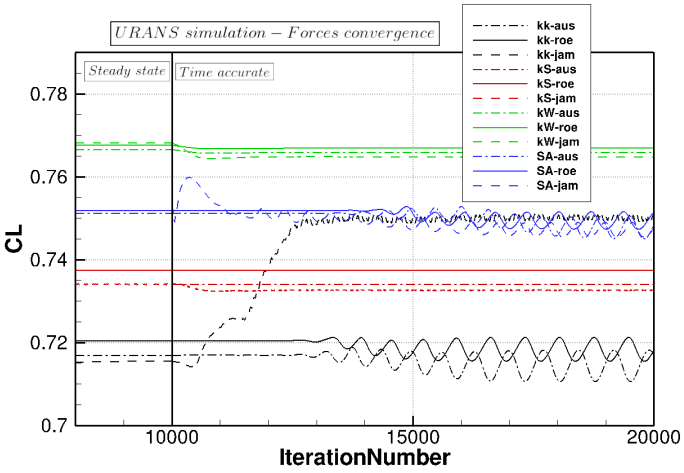

Figure 8 – Evolution of the lift coefficient for time-accurate simulations using different turbulence models and numerical schemes

A link has been found between the convergence of the inner-iteration residual and the prediction of shock oscillations. This is the case for both S-A and k-kL turbulent models, but only with AUSM+P and Roe schemes. When oscillations are observed, the buffet main frequency is relatively close for all cases. Strouhal numbers, computed using the mean aerodynamic chord and the velocity normal to the leading edge, are consistent with values found in the literature (0.2 to 0.6) and are as expected higher than typical values for the 2D phenomenon (0.06).

The time-averaged values of the lift coefficient are most of the time close to the values obtained using steady-state simulations and show a dependency on the turbulence model rather than the numerical scheme. Figure 9 shows the pressure distribution on the CAT3D for the S-A simulation with AUSM+P scheme during a buffet cycle. Each plot in figure 9 corresponds to the instantaneous result of the time-accurate simulation, showing the flow field at a different time step.

The plots allow observing the shock motion during a buffet cycle and showing that the 3D buffet differs from the 2D phenomenon, characterised by a chord-wise oscillation of the shock position. In the 3D case, the unsteadiness also consists in a chord-wise oscillation of the shock position, but this oscillation begins at a position near the middle of the wing and then propagates to the wing tip, thereby creating a wave in the span-wise direction.

In addition to instantaneous results, URANS simulation can be used to extract time-averaged results. Figure 10 shows the average Cp distribution at different span-wise locations for the combinations of turbulence models and numerical schemes able to reproduce the buffet unsteadiness.

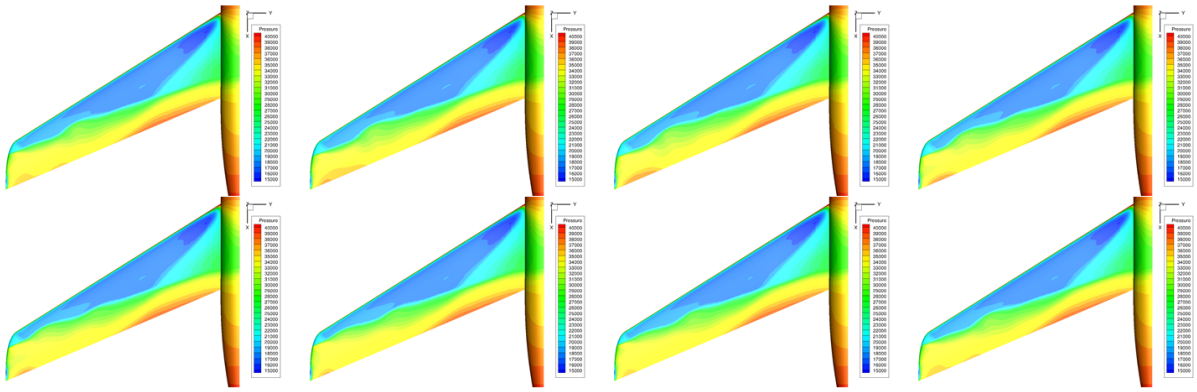

Figure 9 – Pressure distribution for a time-accurate simulation. Instantaneous results at different time steps

The Cp distribution obtained with time-averaged results of URANS simulations yield a better agreement with experimental data than the ones predicted by steady simulations. The main differences appear in the wing tip region (y/b = 72.5% and y/b = 90%) where the evolution of pressure contours reveals important fluctuations. Instead of predicting a sharp pressure drop as it was the case for steady state computations, time accurate simulations compute a more gradual pressure increase between approximately x/c = 20% and x/c = 40%. This feature is also visible in figure 9, where the instantaneous Cp distribution indicates the presence of a sharp pressure jump that evolves in time.
In addition to time-averaged results, URANS simulations can also be used to extract the Root Mean Square (RMS) value of the pressure, which is a convenient way to identify the presence and the intensity of flow unsteadiness.
Figure 11 presents on the left the RMS of pressure over the wing: high values of Prms appear in the wing tip area in the shock region and are related to the fluctuations of the shock location (the pressure fluctuating between the values upstream and downstream of the shock). Downstream of the shock, in the trailing edge region, substantial pressure fluctuation values are predicted because of boundary layer separation where unsteady phenomena exist.
The right side of figure 11 shows the distribution of pressure fluctuations at a constant span-wise location, compared with experimental data. The peak in the computed Prms distribution is predicted downstream the location measured in the wind tunnel test, where a clear peak does not appear but Prms increases when getting close to the shock location. Additionally, RMS values of pressure in the separated zone, downstream of the shock, are under predicted by the URANS approach.

Sensitivity of the time-accurate simulation to numerical parameters

As done in the previous section for the steady-state simulations, the influence of some parameters has also been investigated for the time-accurate simulations. The influence of the Harten correction could have a big impact on the result of a simulation with the elsA solver, which relies on the Roe scheme for the turbulent equations regardless the numerical scheme for the conservative variables. However, it has been found that that this parameter does not have a significant impact on the buffet simulation. On the contrary, when using the second order for the spatial scheme, simulations using Spalart-Allmaras model (that successfully predicted buffet characteristics when a first order discretisation was used) fail to reproduce the phenomenon. Concerning the spatial discretisation, multigrid approach can help the convergence of a simulation. Finally, time-accurate simulations were also performed on a case where the turbulent transition was triggered as in the experimental campaign. Cp distributions, not presented here, allow drawing similar conclusion as for the steady-state simulations (i.e. transition point has a limited influence on pressure distribution and the laminar region moves the shock to a slightly more rearward position).
Finally, the influence of the wing deformation was also evaluated for time-accurate simulations. As for the steady-state solution, the wing tip is impacted more than the wing root. Taking into account the effect of the static deformation of the wing does not enable to improve consistency of the time

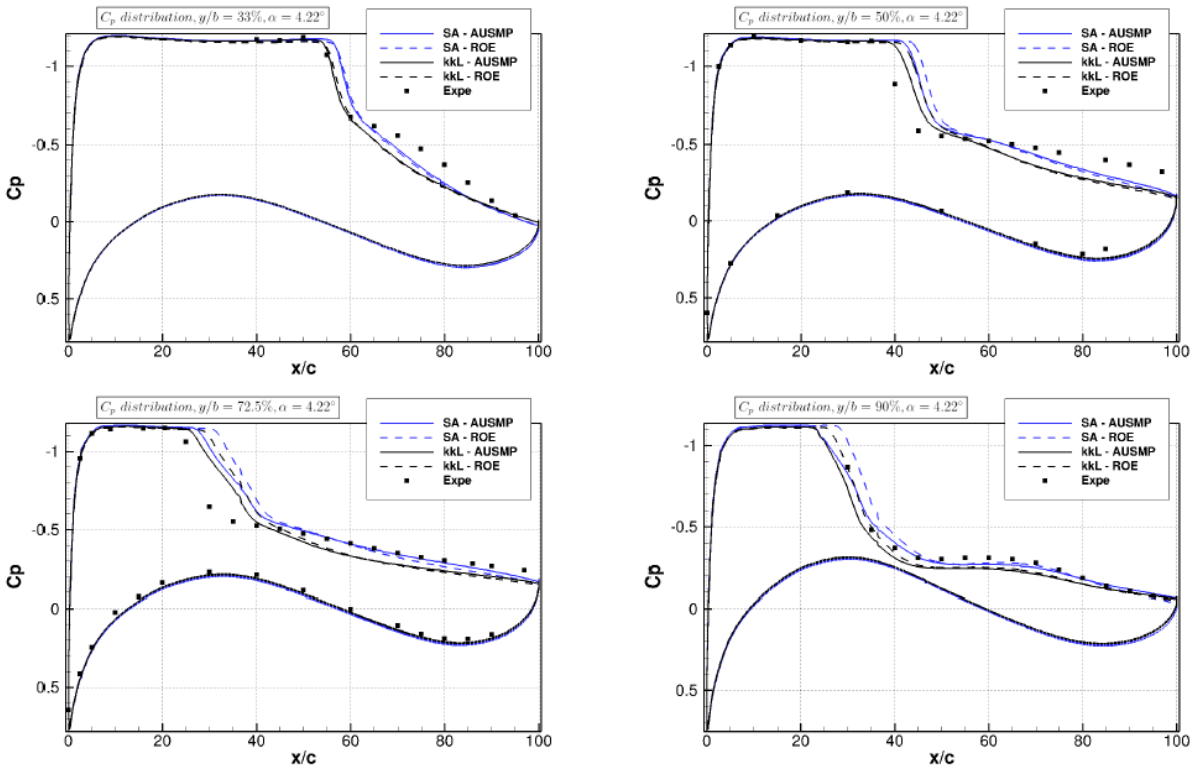

Figure 10 – Pressure coefficient distribution at different span-wise locations, comparison between different time-averaged URANS results and the experimental data

accurate results with experimental data.

4. Results of the ZDES simulations

The objective of this section is to resume the results of the preliminary ZDES simulation on the CAT3D model, performed to assess the capability of the latest enhancement of the ZDES mode 2 [17] developed by ONERA to reproduce transonic buffet. Since the scale-resolving simulations need a fine grid, the first step is the refinement of the mesh presented in the previous section by means of the Chimera technique. Then RANS and URANS simulations were conducted to validate the new configuration against the results on the coarse grid and the experimental data. Then, ZDES simulation were carried out and the results are discussed. Instantaneous, time-averaged and statistics of the flow field obtained with this approach are discussed at the end of this section.

4.1 ZDES grid

Hereafter the grid used in the previous sections for RANS and URANS simulations will be referred to as the “baseline” grid. For the ZDES, a “refined” grid will be used, allowing the resolution of turbulence in the separated region. The refined grid has been obtained by overlapping via the Chimera technique a refined box, created using Pointwise grid generator. As for the previous simulations, the preparation was carried out using the in-house software Cassiopée, developed at ONERA [18], which allows for the setup of the Chimera calculation. Using this technique, multi-zonal overlapped grids are considered in the same simulation. This approach can be very convenient for complex geometries, especially if some parts are moving.

This secondary grid will be referred as Chimera Box and is illustrated in figure 12. So as to enable this superimposition, a delimiter that defines the grid part that was to be computed and the one that has to be masked. Masked points are not calculated, while inter-grid communications are facilitated through data interpolations performed by the solver.

When performing a ZDES, the grid should be fine enough to allow the resolution of the turbulent structures in the separated region. The thickness of this region can be characterised by the vorticity thickness. According to best practices, a minimum amount of grid points is needed in the shear layer.

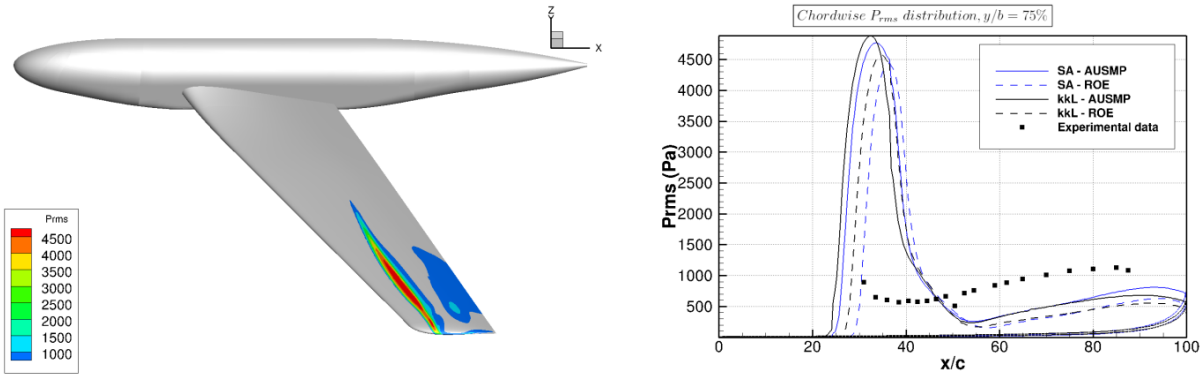

Figure 11 – RMS of pressure. Distribution on the wing surfaces and slice at y/b = 72.5% vs experimental data

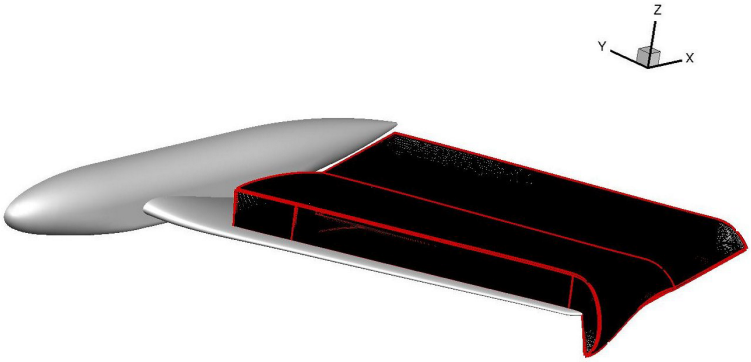

Figure 12 – Chimera box containing the refined grid for the ZDES simulation

This means that the cell size should not exceed the vorticity thickness divided by 15 or 20 in the direction normal to the shear layer (vertical), and divided by 3 in the other two directions. The total number of cells of the refined grid is 93.5 million, split and distributed to be computed on 560 cores.

4.2 Validation

RANS and URANS simulations were performed again on the refined grid to assess grid dependency. No significant differences were observed between the two grids. Before discussing the results obtained with the ZDES technique, in this section some validations of the approach are proposed in order to ensure that the turbulence-resolved simulation is correct. This validation procedure has been performed multiple times during the so-called “transient” simulation, that is when the ZDES is considered to yield preliminary results since the flow unsteadiness and the resolution of turbulence is not fully developed. Once the transient is over, the ZDES is properly running and the statistics can be extracted, as discussed in the next section.

The result of a URANS simulation has been used as a starting point for the ZDES. When moving to the scale-resolving simulation, the time step was lowered to 1e-7 seconds. The Gear method is still used for the temporal discretisation, but 6 inner iterations are sufficient to reach convergence between different time steps. This small time step allowed for maximum CFL values of 60 in the smallest grid cells. Despite this small value, it was not possible to use a high-order low-dissipation scheme: as a consequence, the AUSM+P scheme with the van Albada limiter was kept for the whole ZDES simulation.

A fundamental step for the validation of ZDES results is the analysis of the ratio between the eddy viscosity due to the modelled turbulence and the molecular viscosity. High values of this ratio indicate that the flow is modelled and the turbulence is thus not resolved. Figure 13 shows two instantaneous results, one at the beginning of the ZDES simulation, the second when the transient is over.

The large values of eddy viscosity, typical from RANS modelling, are convected downstream and its value decreases. This indicates that the model has identified a separated region which will be treated

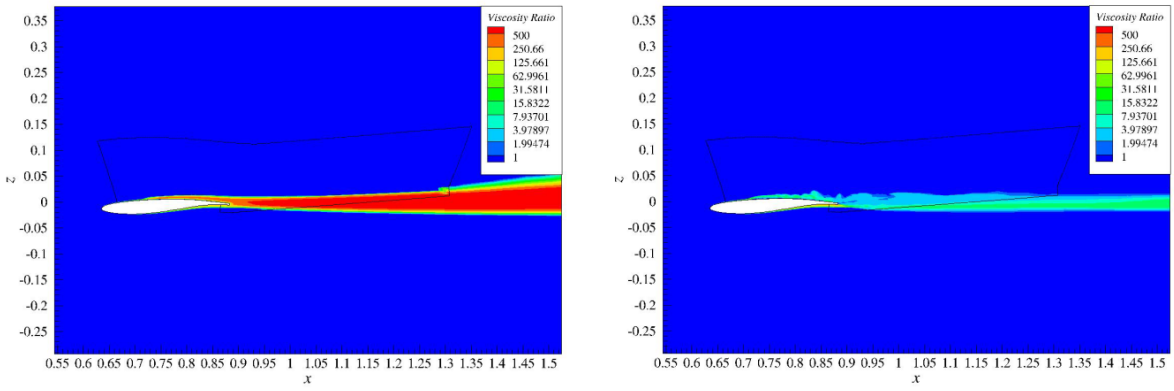

Figure 13 – Eddy viscosity ratio at y/b = 90.0% at the beginning of the ZDES (left) and at the end of the transient (right)

in LES and it has started to resolve the turbulence. Low values of eddy viscosity indicate that the ZDES is behaving correctly and most of the turbulence is resolved and not modelled.

4.3 Results

While the simulation was running, the instantaneous results were monitored in order to validate the ZDES results. The velocity field can be used to visualize the locations of the supersonic and subsonic regions, as well as other features such as the separation of the boundary layer. Figure 14 present the velocity contours for a slice in the x-z plane at y/b=72.5% at a given time instant (t = 0.034 s, corresponding to the black circle in the time-history plot). On the right, the evolution of the lift coefficient indicates that in this instant the shock is in a upstream position. The shock wave causes the detachment of the boundary layer, and the separated zone is visible downstream the shock foot. Turbulent structures, with low values of velocity, are visible in blue from the separated point to the trailing edge and continue further downstream in the wake. On the suction side of the wing, due to the existence of a shock wave, supersonic and subsonic regions delimited by the shock are expected. A sonic region right after the shock can also be seen. During the shock's downstream excursion that will happen after the instant represented in figure 14, the flow is accelerated over the wing, enlarging the supersonic region and strengthening the shock. Once the shock is in its most downstream position, the boundary layer suddenly strongly detaches due to the pressure gradients, pushing the shock upstream. As a result, the chord-wise length covered by the detached boundary layer increases, prompting the decrease of the lift. On the contrary, when the shock is moving upstream, the boundary layer tends to reattach, decreasing the separated region and allowing a new downstream excursion of the shock.

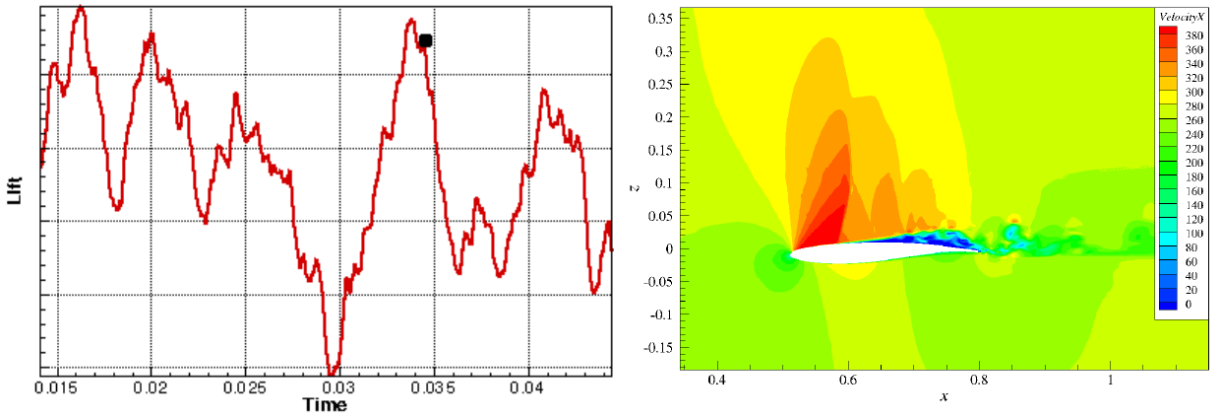

Figure 14 – Time-history of lift coefficient (left) and stream wise velocity field (right) for the instantaneous results corresponding to the dot on the time-history plot

Even if the lift oscillation shows some periodicity and buffet cycles can be identified, the time-history of the signal reflects the rich frequency content of the flow unsteadiness. For this reason, it is useful to compute the time-averaged quantities on several buffet cycles, as performed hereafter. As for the time-accurate URANS simulation of the previous section, this average allows the comparison with the steady Cp and root-mean-square values of the experimental values.
Figure 15 presents the pressure fluctuations on the wing (left side) as well as the chord-wise distribution at y/b = 75%. The highest RMS values are located in a thin strip that starts at about 44% of the wingspan until the wing tip. Within this strip, the highest values are concentrated in the region closer to the leading edge, from 60% to 72% and the maximum is located at 67%. It should also be noted that this strip presents higher curvature as well as overall lower values as the pressure RMS yielded by the URANS simulation. Regarding the high values downstream the shock, these correspond to the fluctuations of the strong separated region, which extends approximately from 44% to 80% of the wingspan. It should be noted that the distribution of these fluctuations depends on the span-wise location. Further to the tip, the boundary layer reattaches. Despite reattachment, there is another small separation at about 90% of the wingspan with relatively high fluctuation values.

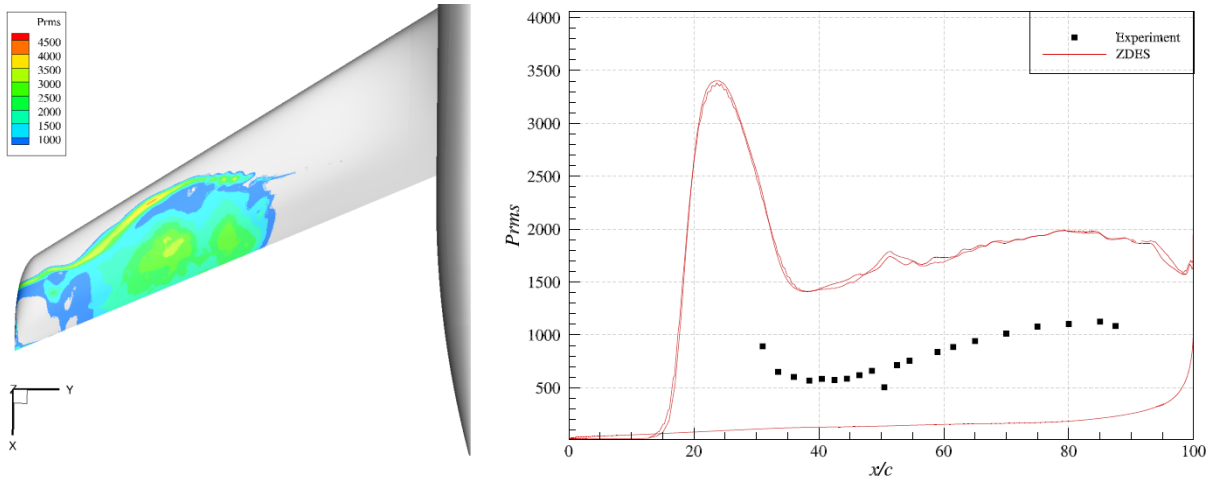

Figure 15 – RMS of pressure on the wing (left) and comparison between ZDES and experiments at y/b = 75%

In order to have a better insight about the accuracy of the fluctuation intensity, pressure RMS distributions at the same locations as the unsteady taps used in the experimental campaign were extracted. As illustrated on the right side of figure 15, the fluctuations in the separated region are higher than the experimental data, suggesting an overestimation of the eddies energy by the ZDES. In other studies at ONERA, it has been found that coarse grids in the normal direction could lead to an overestimation of pressure RMS values due to a too large turbulence scales. Additionally, the AUSM+P scheme could be too dissipative for the model, prompting larger eddies with higher energy. This is consistent with the instantaneous results presented in the previous section.
The left side of figure 16 shows an instantaneous result of the Q-criterion, allowing for a visualisation of the eddies over the wing contributing to the fluctuations of pressure. It is possible to observe that in the region after 33% large eddies are being shed downstream. The size of these structures is large for span-wise positions between approximately 55% and 75%. The wing-tip vortex due to the lifting surface is also visible. Regarding the vorticity close and above the leading edge, this might be caused by the change in cell size due to the existence of the refined region.
The right side of figure 16 shows the Power Spectral Density of the lift signal obtained during the ZDES simulation, after the transient phase. Due to the computational and time constraints, it was not possible to have a longer time history, and consequently the spectrum has a poor frequency resolution. The available spectral experimental data corresponds to a signal recorded by transducers at different span-wise and chord-wise locations. Those Kulite sensors provide the local pressure fluctuations on a given wing position. Since in the simulation only the total lift has been extracted, all the experimental results were plotted together against the simulation results for a qualitative comparison.

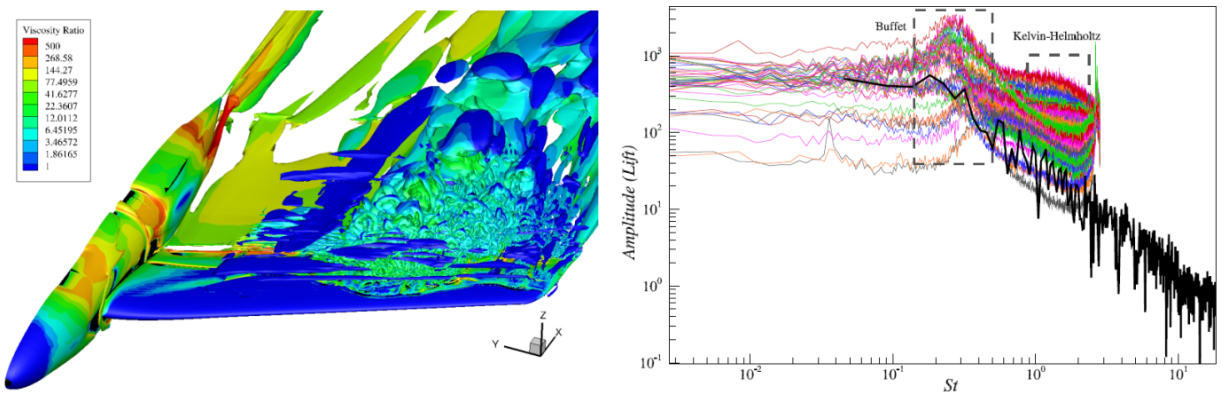

Figure 16 – Q-criterion isosurface of an instantaneous result (left) and Power Spectral Density of the lift coefficient vs the experimental data

The thicker black line, corresponding to the ZDES spectrum, has a minimum resolved frequency higher than the experimental one. This is due to the short duration of the simulation. On the other hand, the simulation maximum resolved frequency is higher than the experimental one given its higher sampling rate. These higher frequencies could be attributed to the small turbulent scales of the eddies in the separated region, as illustrated in the pressure distribution within a buffet cycle. With regards to the Strouhal number associated to the 3D transonic buffet, it can be clearly seen that for the experiment it is mainly concentrated between Strouhal numbers of 0.1 and 0.5. Even though the simulation does not present a rich content within this interval, it is worth noticing that the two main dominant peaks at Strouhal numbers of 0.18 and 0.32 belong to this range. Hence, it can be concluded that ZDES achieves to replicate the periodic motion of the 3D transonic buffet.

5. Comparison between the different approaches

This section presents a comparison between the results obtained using different approaches presented before. As mentioned in section 3.3 , the low angle of attack case does not present any unsteadiness. For this reason this case has not been investigated by means of ZDES. The absence of unsteadiness found by the time-accurate simulation yealds the same results between RANS and URANS, so it will not be discussed in this section. On the contrary, the high-angle of attack case not only presents differences between steady-state RANS and time-accurate URANS, but has also been investigated in ZDES.

The results of the time-resolved simulations have been time-averaged in order to allow the comparison between each other and with the steady-state RANS results. In order to ease the comparison between the turbulence-modelling and turbulence-resolving approaches, only the Spalart-Allmaras turbulence model is discussed for the RANS and URANS simulations. In addition, the numerical scheme is also kept the same in this comparison, so that all results discussed hereafter have been obtained with the same AUSM+P numerical scheme.

Figure 17 presents a comparison of the Cp distributions at all available span-wise stations for the case at high angle of attack (α=4.22^o). Time-averaged ZDES results, obtained on a finer grid as described in section 4.2are also included in the same plot. Similar plots with more details of the results obtained with different models and schemes have been presented in figures 5 and 10 for RANS and URANS, respectively.

The first of the four plots in figure 17 presents the Cp distribution at y/b = 33%. Close to the fuselage RANS and URANS are identical, indicating that no low-frequency unsteadiness is present in this region. The blue line, corresponding to the ZDES result, can however achieve a more satisfying agreement with the experimental data in terms of shock location. The flow deceleration downstream of the shock, associated with an increase of the pressure, remains overestimated by all approaches. The absence of shock motions can be seen also at y/b = 55%, where all approaches predict a sharp pressure increase at the shock location. However the ZDES has a tendency to predict the shock foot too upstream. Downstream of the shock, especially in the trailing edge region, the ZDES provides

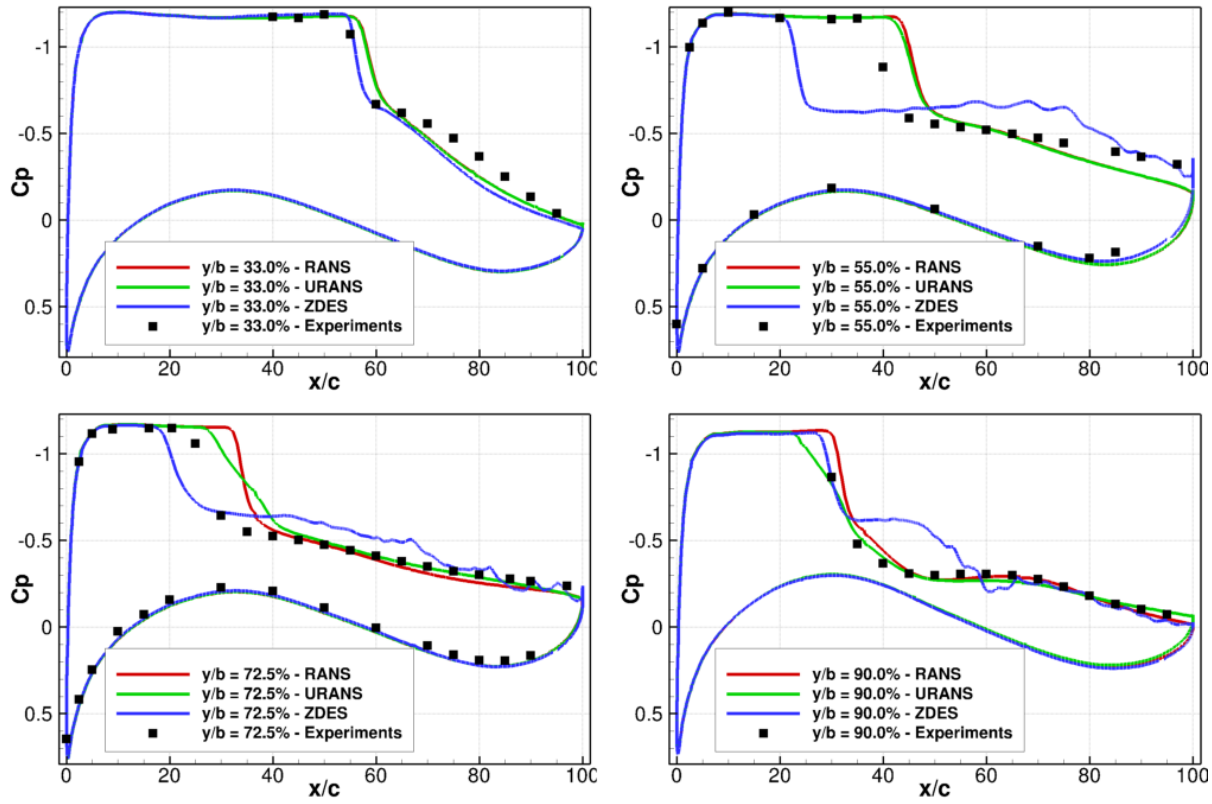

Figure 17 – Time-averaged Cp distribution at α=4.22° for RANS, URANS and ZDES computations

a better representation of the pressure recovery, even if the oscillations on the Cp indicate that the time-averaging is not long enough to provide a statistically converged flow.
A similar behaviour can be observed on the third plot (y/b = 72.5%). However at this location the URANS approach yields the better representation of the separated region. In terms of shock location, the ZDES is once again too upstream, even if the slope of the pressure increase at the shock foot is better predicted than in URANS. At this span-wise location the shock motions are the most energetic, and the red line clearly indicates that a RANS approach is not adapted to capture the flow-physics.
When focusing on the last plot, referred to the location the closest to the wing tip, the shock location is perfectly captured by the ZDES. However the results indicate a second shock, downstream the first one (probably associated with the supersonic tongue visible on the right side of figure 14), not present in the experimental data. In this region the amplitude of the shock motion is limited, so the RANS results predicts a sharp pressure increase that is not far from what was measured in the experiments.
The analysis of the Cp distribution allows for a fair comparison between the approaches. However, one should not forget that each simulation has its own advantage and drawback. For example the RANS simulation, despite not being able to reproduce the unsteadiness, provides a fair agreement with the experimental data with a very low computational cost. On the other side, the more expensive ZDES, even if it presents some discrepancies with the experimental results, provides a solution with much more information about the flow physics, like for example the frequency content or the fluctuations. Finally, as mentioned before, part of the discrepancy of the ZDES results is probably due to the too short duration of the simulation due to the available resources.

6. Conclusions

This work has focused on the analysis of the transonic buffet by numerical means on the CAT3D model, a half wing-body configuration. First, RANS and URANS simulations were used to assess the capability of these turbulence-modelling approaches to reproduce the transonic buffet phenomenon. RANS results have shown the capability of the steady-state simulation to reproduce the flow-physics when the angle of attack is small. Time-accurate URANS simulations have proved to be able to reproduce the transonic buffet within the limitations of the approach. However, since shock motions

are at low-frequency, it managed to reproduce the periodic shock oscillation typical of the buffet phenomenon. Likewise, it depicted a relatively accurate shock foot position but poor agreement was found in the level of the fluctuations intensity downstream. The overall flow field was in satisfying agreement with the experimental data.
ZDES was then considered and a simulation was run producing a total of 6 transonic buffet cycles. In terms of the ZDES mode 2 quality, it can be said that its protection function behaves as expected, correctly securing the boundary layer and allowing the development of instabilities. Additionally, the grey area between RANS and LES is narrow, prompting a fast switch from one model to the other. Therefore, it can be concluded that the enhanced ZDES mode 2 considered in this study is suitable for transonic buffet simulations.
With regards to the reproduction of the flow field, it was noted that there is an overestimation of the levels of turbulence after the shock. This leads to a prediction of the shock too upstream for those span-wise locations where these fluctuations are most intense. A reason for this could be due to the combination of a dissipative scheme and a too coarse grid. Consequently, it would be interesting to generate a new grid, refined in the normal direction, which could allow the use of less dissipative numerical scheme. Lastly, the simulation should be run for a longer period of time, yielding at least 10 buffet cycles. Nonetheless, within the limitations of this simulation both in terms of grid and computational time, ZDES was able to reproduce the transonic buffet. It yielded a frequency spectrum with two dominant peaks within the expected Strouhal number range and it captures the main flow features related to the shock motion and its induced separation. Additionally, it gave an overview of the location of the strongest fluctuations and, where those were of lower intensity, the shock location matched the experimental results.

7. Acknowledgements

ONERA would like to acknowledge the financial support for the ZDES simulation. The computations were performed on the Occigen cluster of GENCI (Grand équipement national de calcul intensif), under the DARI project number A0082A11338.

8. Contact Author Email Address

The contact author is Fulvio Sartor: fulvio.sartor@onera.fr

9. Copyright Statement

References

[1] Jacquin, L., Molton, P., Deck, S., Maury, B. and Soulevant, D., “Experimental Study of Shock Oscillation over a Transonic Supercritical Profile”, *AIAA Journal*, Vol. 47, No. 9, 2009, pp. 1985-1994

[2] Benoit, B., Legrain, I., “Buffeting prediction for transport aircraft applications based on unsteady pressure measurements”, *AIAA Paper 87-2356*, 1987

[3] F. Roos, “The buffeting pressure field of a high-aspect-ratio swept wing”, *AIAA Paper 85-1609*, 1985

[4] Dandois, J. “Experimental study of transonic buffet phenomenon on a 3D swept wing”, *Physics of Fluids* 28, 2016

[5] Sartor, F., Mettot, C., Sipp, D., “Stability, receptivity, and sensitivity analyses of buffeting transonicflow over a profile”, *AIAA Journal*, Vol. 53, No. 7, 2014, pp.1980-1993

[6] Iovnovich, M., Raveh, D.E., “Reynolds-averaged Navier-Stokes study of the shock buffet instability mechanism”, *AIAA Journal*, Vol. 50, No. 4, 2012, pp. 880-890

[7] Koike, S., Ueno, M., Nakakita, K., Hashimoto, A., “Unsteady pressure measurement of transonic buffet on NASA Common Research Model”, *AIAA Paper 2016-4044*, 2016

[8] Crouch, J. D., Garbaruk, A., Strelets, “Global instability in the onset of transonic-wing buffet”, *Journal of Fluid Mechanics*, 2019, 881, pp. 3-22

[9] Paladini, E., Beneddine, S., Dandois, J., Sipp, D. and Robinet, J.-C., “Transonic buffet instability: From two- dimensional airfoils to three-dimensional swept wings”, *Physical Review Fluids*, 2019, Vol. 4.

[10] Plante, F., Dandois, J., Laurendeau, E., "Similarities between cellular patterns occuring in transonic buffet and subsonic stall", *AIAA Journal*, Vol. 58, No. 1, 2020.

[11] Plante, F., Dandois, J., Beneddine, S., Sipp, D., Laurendeau, E., "Numerical simulations and global stability analyses of transonic buffet and subsonic stall", *Journal of Fluid Mechanics*, Vol. 908, 2020.

[12] Rumsey, C.L, Allison, D. O., Biedron, R.T., Buning, P.G., Mysko, S.J., and Witkowski, D.P., “CFD Sensitivity Analysis of Modern Civil Transport Near Buffet-Onset Conditions”, *NASA/TM-2001-211263*

[13] F. Sartor , S. Timme, “Reynolds-Averaged Navier-Stokes simulations of shock buffet on half wing-body configuration”, *AIAA Paper 2015-1939*, 2015

[14] V. Brunet, S. Deck, “Zonal-Detached Eddy Simulation of transonic buffet on a civil aircraft type configuration”, *Advances in Hybrid RANS-LES Modelling*, Springer, 2008, pp. 182-191

[15] Sartor, F. and Timme, S.“Delayed detached-eddy simulation of shock buffet on half wing-body configuration”, *AIAA Paper 2015-2607*, 2015

[16] Cambier, L. and Plot, S., “The ONERA elsA CFD software: input from research and feedback from industry”, *Mechanics Industry*, EDP Sciences, 2013, 14 (3), pp.159-174.

[17] Deck, S. and Renard, N. “Towards an enhanced protection of attached boundary layers in hybrid RANS/LES methods”, *Journal of Computational Physics*, Volume 400, 2020.

[18] Benoit B., Péron S. and Landier S., “Cassiopee: A CFD pre- and post-processing tool”, *Aerospace Science and Technology*, Volume 45, 2015.